CrossMark

J. Plasma Phys. (2022), *vol*. 88, 905880113 © The Author(s), 2022.
Published by Cambridge University Press
doi:10.1017/S0022377821001367

On the electric field components in the collisionless plasmoid instability

M. Shahraki Pour[1] **and M. Hosseinpour**[1],†

[1]Faculty of Physics, University of Tabriz, PO Box 16471, Tabriz, Iran

(Received 21 September 2021; revised 20 December 2021; accepted 21 December 2021)

Using two-dimensional particle-in-cell simulations of collsionless plasmoid instability, the spatial and temporal variations of electric field components are investigated. The initial magnetic field is a Harris sheet which is added by a non-uniform perpendicular magnetic field (guide field). The effects of weak and medium guide field on the evolution of plasmoid instability and associated electric field are discussed with the input parameters of the solar corona with the condition $\omega_{pe}/\omega_{ce} > 1$. As the current sheet elongates, magnetic reconnection in an X-point transits into the plasmoid instability, in which secondary X-points are formed and the consequent magnetic islands coalesce and form larger islands. During the instability, electric field components show two types of disturbances. (1) Transient waves, being excited very early, propagate mainly perpendicular to the current sheet and become damped as the instability proceeds to the nonlinear stage. Fourier analysis reveals that electromagnetic right- and left-hand polarized modes parallel to the initial magnetic field and also the extraordinary mode perpendicular to the current sheet are excited. Additionally, electron Langmuir and slow magnetosonic waves are observed in both directions. (2) Inside the current sheet, an electric field is generated by the plasmoid-dominated reconnection and grows in amplitude as the plasmoid instability proceeds. Moreover, in our study, the effects of amplitude-varying guide field on the spatial structure of electric field components outside and inside the current sheet are discussed. This study is valuable because understanding the spatial and temporal variation of the electric field is an essential prerequisite for the issue of particle acceleration in plasmoid-dominated magnetic reconnection.

Key words: astrophysical plasmas, plasma simulation, plasma waves

1. Introduction

Plasmoid instability is one of the macroscopic magnetohydrodynamic instabilities, which is caused by the magnetic reconnection process in narrow electric current sheets in magnetized and highly conductive plasmas. Following this basic plasma process, the stored magnetic energy is converted to plasma kinetic and thermal energies by changing the topology of the magnetic field lines (Priest & Forbes 2000; Birn & Priest 2007; Yamada, Kulsrud & Ji 2010; Gonzalez & Parker 2016).

The formation of current sheets in the solar corona is an important open question. Large-scale photospheric motions lead to the formation of coronal current sheets (Galsgaard & Nordlund 1996; Gudiksen & Nordlund 2005). The formation of highly

† Email address for correspondence: hosseinpour@tabrizu.ac.ir

https://doi.org/10.1017/S0022377821001367 Published online by Cambridge University Press

elongated current sheets in coronal magnetic fields would result in extremely low reconnection rates, which fail to account for the observed fast energy release rates. Such current sheets are naturally subject to a violent plasma instability leading to the breakup, fragmentation and formation of multiple current sheets instead of just one monolithic current layer with reconnection occurring at multiple X-points (Loureiro, Schekochihin & Cowley 2007; Cargill *et al.* 2012). The current sheets with a high length-to-width ratio break up into a chain of plasmoids well before the well-known Sweet–Parker aspect ratio is achieved (Comisso *et al.* 2016, 2017). This is an important aspect, especially for the solar corona, where the Lundquist number S is very large ($S > 10^{13}$). Another important point to mention is the open problem of the onset of fast magnetic reconnection in solar corona applications (Bhattacharjee 2004). It is believed that the formation of palsmoid instability in the current sheets can provide an explanation for the impulsive nature of magnetic reconnection in the solar corona.

According to the linear analytical theory of this scenario, a current sheet with a high length-to-width ratio is not subject to the slow well-known Sweet–Parker reconnection mechanism, but it is inherently unstable to the formation of plasmoids on very short time scales. It is therefore clear that for sufficiently large systems, plasmoid-dominated reconnection layers are inevitable. Plasmoid formation and magnetic reconnection are thus inextricably linked, and further progress in understanding reconnection in realistic systems necessarily requires a theory that takes the plasmoid dynamics into account.

The observation of plasmoid structures in the solar atmosphere has already been reported (Bárta *et al.* 2011; Liu, Chen & Petrosian 2013). Formation of such plasmoids (magnetic islands or helical flux ropes in three dimensions) gives rise to the tremendous increase in the reconnection rate and the magnitude of the reconnection electric field. Fragmentation of such a current sheet into smaller structures may offer a more promising way forward, providing not only multiple accelerator sites, but also the presence of microscale turbulence to both confine the particles to the vicinity of the accelerators and provide secondary acceleration.

Plasmoid chains are highly dynamic configurations and grow fast by coalescence of smaller plasmoids (Bhattacharjee, Brunel & Tajima 1983; Daughton *et al.* 2009; Intrator *et al.* 2009; Karimabadi *et al.* 2011). The kinetic perspective of plasmoid chain formation and evolution has been investigated through particle-in-cell simulation by Markidis *et al.* (2012). Also, Drake *et al.* (2006) have studied the formation of secondary islands and shown that the presence or absence of an out-of-plane magnetic field (guide field) has a major effect on the long-term behaviour of magnetic reconnection.

Kumar *et al.* (2019) reported observation of the formation and evolution of multiple small plasmoids with bidirectional flows associated with fast reconnection in three-dimensional breakout current sheets in the solar corona. They demonstrated the existence and importance of plasmoids during fast reconnection in a fully three-dimensional magnetic configuration. Liu *et al.* (2013) showed that the main sites of particle acceleration and plasma heating are in the reconnection outflow regions, rather than the reconnection site itself.

Furthermore, Zhou, Deng & Huang (2012) studied the structure of electric field inside a secondary island in the diffusion region using particle-in-cell simulation without initial guide field. They presented the electric field component diagrams at a particular time and showed that intense in-plane electric fields, which point towards the centre of the island, form inside the secondary island and the magnitudes of the in-plane electric fields inside the island are much larger than those outside the island in the surrounding diffusion region. Also, they found electric dipole structure by the electric field components.

Fan *et al.* (2016) compared the structure of primary and secondary magnetic islands through particle-in-cell simulation and discussed the values of different components of the

https://doi.org/10.1017/S0022377821001367 Published online by Cambridge University Press

electric field in different parts of the primary and secondary islands. Also, they concluded that the out-of-plane magnetic field can be enhanced in the centre of both the primary and secondary islands. According to their results, the magnitude of the electric field components in the O-points is greater than in the X-points.

On the other hand, Chen *et al.* (2012) studied in-plane electric fields in secondary and primary islands by particle-in-cell simulations, and compared the results with spacecraft measurements from the Earth's magnetotail. They found that in-plane electric field components are locally peaked around the secondary island cores.

Moreover, Fu *et al.* (2018) by examining the structure of out-of-plane electric field with different guide field coefficients at a specific time in the X-point of magnetic reconnection concluded that a guide field coefficient higher than a specific value will cause the Hall electric field to be replaced by a tripolar electric field. Wan *et al.* (2008) investigated the time evolution of the electric field component perpendicular to the reconnection plane at the X-point and showed that the energetic electrons were accelerated by the perpendicular component of electric field. They stated that the perpendicular component of the electric field has a monopolar structure in early times and a bipolar structure in later times. Egedal, Daughton & Le (2012) used two-dimensional kinetic simulation without guide field and showed that during reconnection, powerful energization of electrons by magnetic-field-aligned parallel electric field can occur over spatial scales that exceed those of previous theories and simulations. Also, the fine magnetic structure of plasmoids generated during reconnection in the presence of guide field was addressed by Karimabadi, Krauss-Varban & Omidi (1999).

Reconnection-generated electric field is the direct agent of charged particle acceleration to relativistic energies in space and astrophysical plasmas, especially in the solar corona. Therefore, the corresponding study of excited waves and their spatial and temporal variations in plasmoid-dominated reconnection (plasmoid instability) is important. Most of the related analytical and numerical works have considered the issue of magnetic reconnection in an X-point or a Sweet–Parker layer. However, the effect of non-uniform guide field with varying amplitude on the electric field has received less attention. Therefore, it is of interest for us to study the spatial and temporal variation of different components of the electric field during the collisionless plasmoid instability with the presence of non-uniform weak and medium guide fields. To understand the nature of disturbances in the electric field components, their respective dispersion diagrams are obtained and analysed. To do so, we employ two-dimensional particle-in-cell simulations. The paper is organized as follows: § 2 describes the simulation set-up, which is followed by presentation and examination of the results in § 3. Summary and conclusion are given in § 4.

2. Simulation set-up

The initial magnetic field is a combination of a reconnection plane xy component and an out-of-plane guide field in the form $\boldsymbol{B} = B_0 \tanh((y - L_y/2)/\delta)\hat{e}_x + b_{z0}\,\mathrm{sech}((y - L_y/2)/\delta)\hat{e}_z$. Here, B_0 and b_{z0} are the amplitudes of the initial magnetic field and the guide field, respectively, L_y is the simulation box size in the y direction and δ is the half-width of the initial current sheet. In order to facilitate the onset of collisionless magnetic reconnection in the centre of the simulation box ($x = L_x/2$, $y = L_y/2$), a divergence-free small perturbation $\boldsymbol{b}_p = b_{px}\hat{e}_x + b_{py}\hat{e}_y$ is added to the initial magnetic field.

The total magnetic field is embedded in a collisionless hydrogen plasma with reduced mass ratio $m_i/m_e = 100$, and the uniform temperatures of electron and ion species are set to be $T_e = 200$ eV and $T_i = 0.25T_e = 50$ eV. The use of a non-physical mass ratio due to computational limitations has been considered in some relevant reconnection

https://doi.org/10.1017/S0022377821001367 Published online by Cambridge University Press

works. Considering the nature of modes discussed below, taking into account the physical mass ratio for hydrogen plasma will not result in the generation of new kinds of waves, but will result in the very late excitation of ion-related modes. Moreover, the initial density of both species is $n_i = n_e = n_0(1 + \gamma\ \mathrm{sech}^2((y - L_y/2)/\delta))$, where $\gamma = b_{z0}^2/B_0^2 - 1$ and $n_0 = 10^{13}\ \mathrm{m}^{-3}$. Therefore, the electron plasma frequency with considering n_0 is $\omega_{\mathrm{pe}} = 0.18$ GHz. Collisions between all particles are neglected in the simulations. The mostly used approximation of collisionless plasma is an initial assumption based on the fact that our study considers a dilute (low-density) region of the solar corona where it is believed that the average Coulomb collision frequency between particles is less than the electron plasma frequency.

Two-dimensional (2D3V) electromagnetic particle-in-cell simulations are carried out using the EPOCH (Extendable PIC Open Collaboration) code, developed at the University of Warwick. The size of the simulation domain is $L_x = L_y = 18.5d_i$, with $d_i = c/\omega_{\mathrm{pi}}$ as the ion inertial skin depth. Also, the number of grid points is $N_x \times N_y = 1000 \times 1000$, so the spatial resolution is $\Delta x = \Delta y = 0.02d_i$. The time step being determined by the Courant–Friedrichs–Lewy condition is $\Delta t = 6.12 \times 10^{-10}$ s, which is sufficiently small to precisely detect the excited waves in the system. We employ 100 particles per species per cell. Due to the computational limitations, it was not possible to run the simulations with larger number of particles. However, we were able to run only one simulation with physical mass ratio $m_i/m_e = 1836, Nx \times Ny = 1500 \times 1500$ and 500 particles per species per cell for the case $b_{z0} = 0.3B_0$ using the High Performance Computing facility of the Sharif University of Technology (Tehran, Iran), but found no significant differences in the dispersion diagrams. This result makes us more confident about our results presented here. Having taken the solar corona parameters, we set $B_0 = 0.001T$, $b_{z0} = 0.3B_0, 0.5B_0, 0.7B_0$ and $\delta = d_i$. Furthermore, for both fields and particles, respectively, the periodic and conducting boundary conditions are applied in the x and y directions.

3. Simulation results

The initial magnetic field has a guide field component which depends on the 'y' direction as $b_z = b_{z0}\,\mathrm{sech}((y - L_y/2)/\delta)$. Its amplitude is set to be $b_{z0} = 0.3B_0$, $0.5B_0$ and $0.7B_0$ ($b_{z0} < B_0$) in three distinct simulation Runs A, B and C, respectively. The only difference between the three runs is the value of b_{z0}. For Run A (weak guide field), figure 1 shows the magnetic field lines at times $t\omega_{\mathrm{pe}} = 50$, 500 and 1500. Figure 1 illustrates how the plasmoid instability develops in the system. Initially, reconnection is triggered at the X-point near the centre of the current sheet ($x = y = L_x/2$). Then, following the thinning of the reconnecting layer at early times, some secondary X-points are formed (linear stage), and, as instability evolves, the generated magnetic islands grow in size and coalesce with each other, forming larger islands with sizes even greater than the initial current sheet. Merging of islands continues until the saturation regime is reached. In other words, at this nonlinear stage, the current sheet is fragmented considerably and a fully nonlinear plasmoid instability has been set up in the system, where all main quantities such as perturbed electric/magnetic fields are completely nonlinear. Such a drastic fragmentation of the current sheet at longer times changes the topological and dynamical structure of the simulation region. The electric current density inside magnetic islands (O-points) is larger than that at X-points as the magnetic field gradients are stronger there.

Now, it would be of interest to look at the way that the different components of the electric field evolve during the growth of plasmoid instability in our system. Since

https://doi.org/10.1017/S0022377821001367 Published online by Cambridge University Press

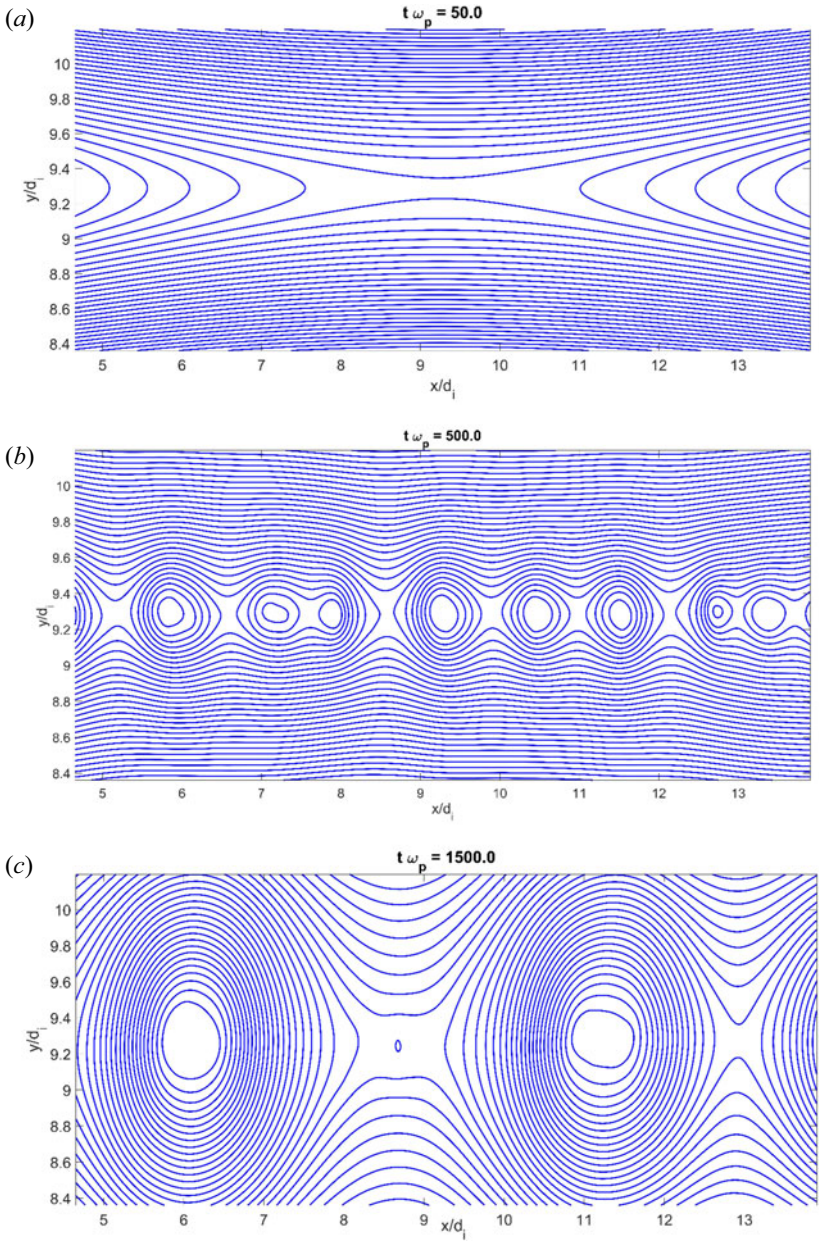


FIGURE 1. The magnetic field lines at times $t\omega_{\rm pe} = 50$ (*a*), 500 (*b*) and 1500 (*c*) with $b_{z0} = 0.3B_0$.

the electric field is responsible for acceleration of charged particles, understanding its evolution in space and time is important.

Figures 2 and 3 show the E_x and E_y components of the electric field on the reconnection plane, xy, at $t\omega_{\rm pe} = 50$, 500 and 1500. According to figures 2 and 3, two distinct types of disturbances can be distinguished. (1) There exist field perturbations originating very early at a few $t\omega_{\rm pe}$ from the current sheet and propagate perpendicularly away from the current sheet along the y axis. These disturbances are mainly y-dependent. As time passes,

https://doi.org/10.1017/S0022377821001367 Published online by Cambridge University Press

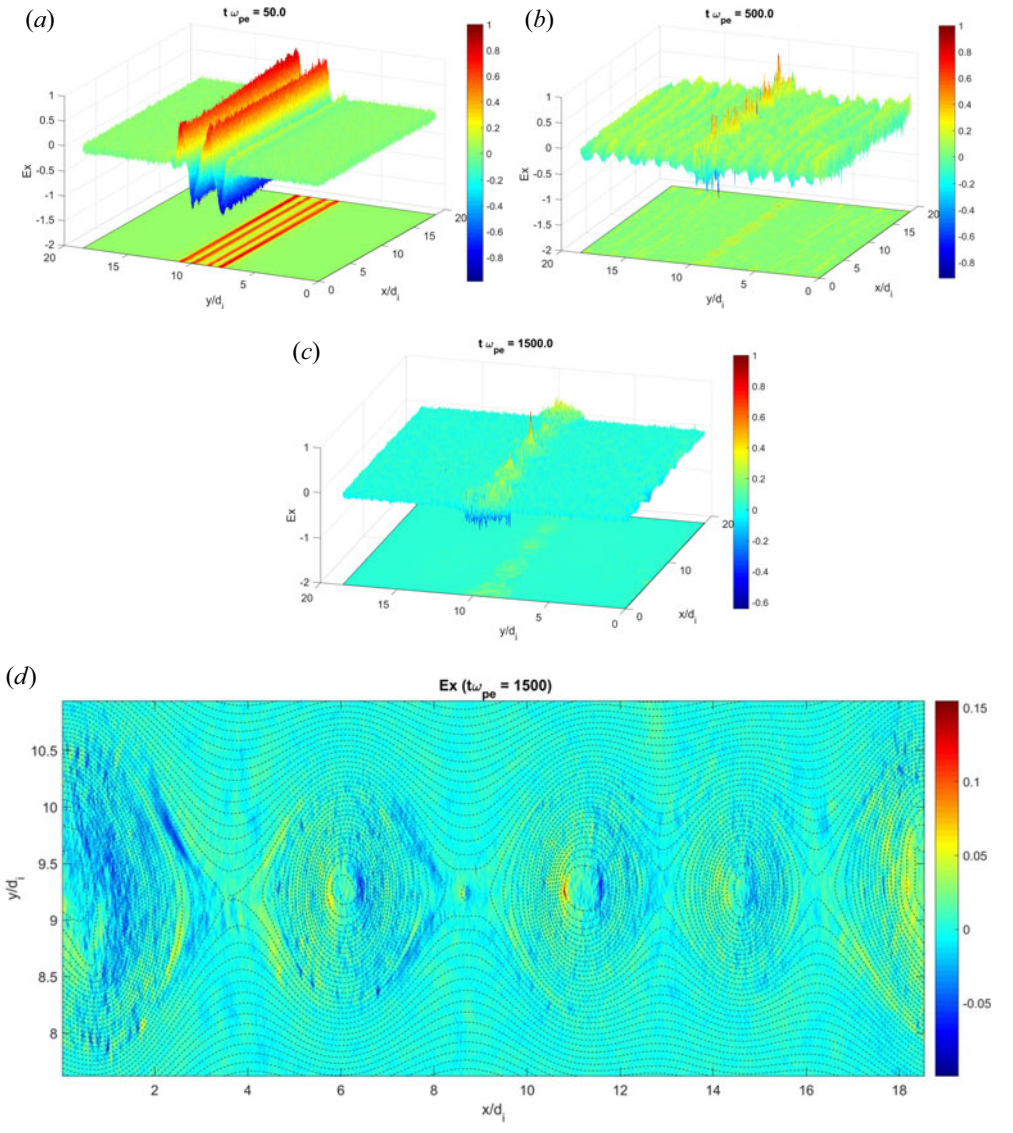


FIGURE 2. The E_x component of the electric field at times $t\omega_{\rm pe} = 50$ (*a*), 500 (*b*), 1500 (*c*) and 1500 (zoomed-in) (*d*) with $b_{z0} = 0.3B_0$.

the growth of an instability along the x axis makes the structure of the disturbances non-uniform along the x axis too, which means that the wavenumber vector has at least both components k_x and k_y. Meanwhile, both the amplitude and the dominant wavelength decrease in time. In other words, k_x and k_y shift to larger values. At $t\omega_{\rm pe} = 50$ the maximums of E_x and E_y are 15 and 18 kV m^{-1}, respectively, which decrease almost five times at $t\omega_{\rm pe} = 1500$. The amplitude of the initial magnetic field B_0 determines how large the electric field would be. To see this point, a run (not reported here) with a magnetic field 10 times weaker, $B_0 = 10^{-4}$ T, was done which showed that the maximum of the electric field reduces to below 1 kV m^{-1} at $t\omega_{\rm pe} = 50$.

https://doi.org/10.1017/S0022377821001367 Published online by Cambridge University Press

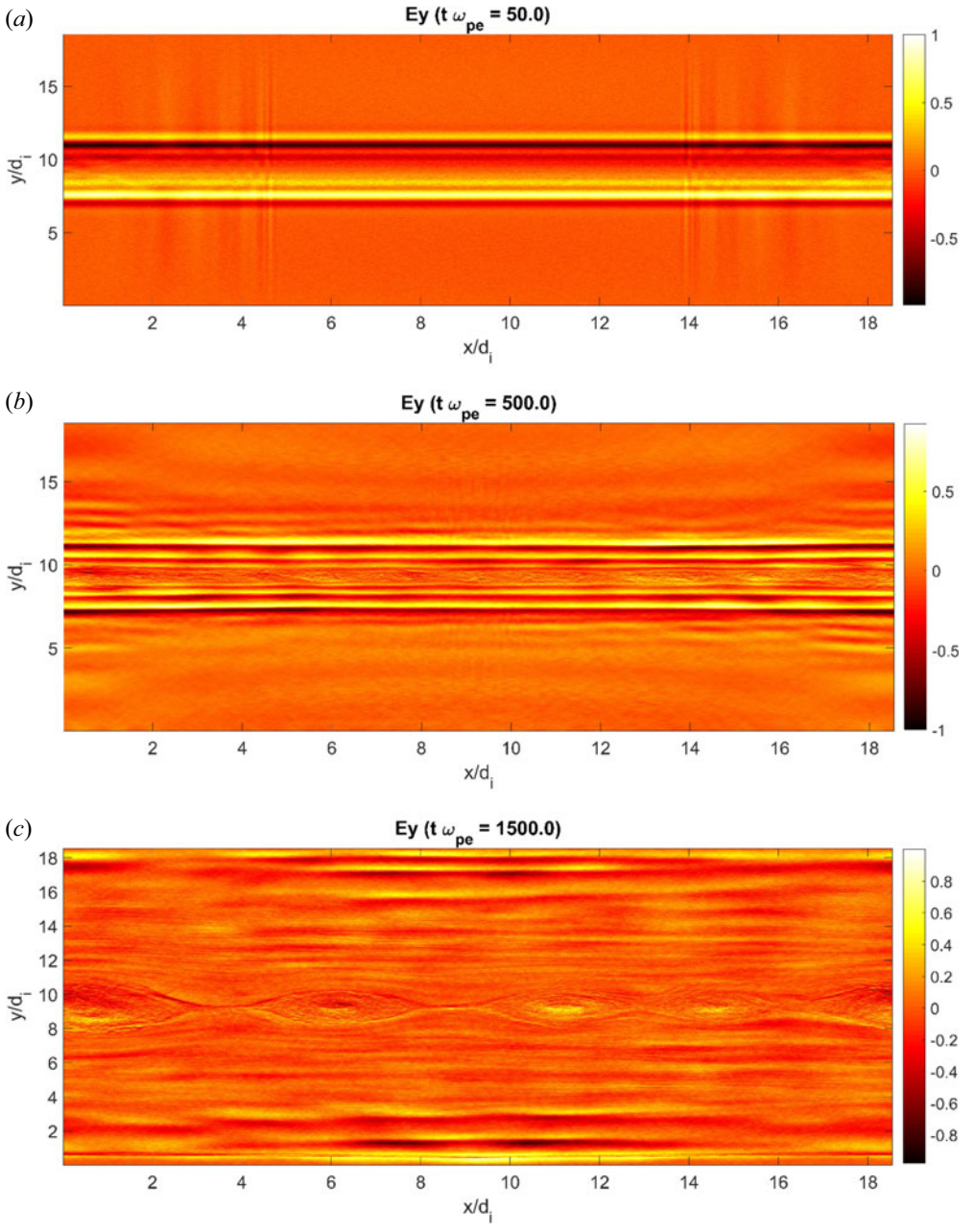


FIGURE 3. The E_y component of the electric field at times $t\omega_{\rm pe} = 50$ (*a*), 500 (*b*) and 1500 (*c*) with $b_{z0} = 0.3B_0$.

Similar patterns of disturbances are also observed for B_x and B_y components of the perturbed magnetic field. The nature of these oscillations, either electrostatic or electromagnetic, is discussed below by implementing spatial and temporal Fourier analysis. It should be noted that such types of disturbances appear for Runs B and C for which the amplitude of the guide field is larger (medium guide field). It can be said that the nature of these disturbances is indeed independent of the formation and

https://doi.org/10.1017/S0022377821001367 Published online by Cambridge University Press

evolution of plasmoid instability taking place initially inside the current sheet, although these disturbances can be affected later by the nonlinear stage of the plasmoid instability. These disturbances are transient waves that propagate away from the current sheet with a large group velocity (see below) and are gradually damped. In particular, the wave-like perturbed electric field in the xy plane is less effective in accelerating charged particles compared with the same role that can be played by an almost DC electric field generated during the magnetic reconnection and consequent plasmoid instability. So, at longer time scales the transient part of the electric field becomes ignorable.

(2) As the reconnection is triggered, electric field is generated inside the current sheet and the subsequent transition of reconnection into the plasmoid instability is accompanied by the amplitude growth of different components of the electric field there. According to figures 2 and 3, as the plasmoid instability evolves and develops in time, its associated electric field grows too and its components become larger. At longer times $t\omega_{\rm pe} > 1000$, the electric field perturbations inside the current sheet are predominant over the electric field disturbances of transient waves outside the current sheet. The in-plane electric fields within magnetic islands closer to the O-points and also around separatrices are considerably stronger than those at the X-point regions. Additionally, E_x and E_y show dipole field structures inside magnetic islands. Inside magnetic islands, the electric field vector rotates around the O-points, and the electric field reverses its direction over the separatrices. The maximums of E_x and E_y inside the islands at $t\omega_{\rm pe} = 1500$ are 45 and 30 kV m^{-1}, respectively. Generally speaking, the electric field supported by reconnection and subsequent plasmoid instability lasts for much longer times and is larger and hence, as far as the particle acceleration is concerned, more attention should be paid to that compared to the electric field disturbances generated by transient waves.

In the scenario of particle acceleration perpendicular to the reconnection plane, the role of out-of-plane electric field, E_z, generated by reconnection, is essential. The previously described transient disturbances have also been observed here. The disturbances, however, are uniform in the x direction, but as time increases, they become non-uniform structures in both directions since the k_x component of unstable waves becomes comparable to the k_y component. Unlike the E_x, E_y plots, disturbances there exist and dominate especially close to the y-axis boundaries even at longer times. Presumably, an electromagnetic mode supporting E_z is still propagating in the system. The maximum of E_z at $t\omega_{\rm pe} = 1500$ is 12 kV m^{-1} which is smaller than the maximums of E_x and E_y at that time. In figure 4, we show zoomed-in plots at different times $t\omega_p e = 374$, 500 and 1000 for $b_{z0} = 0.3B_0$. As seen, the E_z variation in the xy plane is correlated with the plasmoid dynamics. The out-of-plane electric field generated by magnetic reconnection, E_z, is significant at the X- and O-points. However, the magnitude of E_z in the vicinity of X-points is larger than that in the O-point regions. As time increases (instability evolves), the magnitude of E_z also increases. However, as instability develops, the E_z structure becomes complicated. Therefore, we conduct spatial (two-dimensional) and temporal Fourier analysis of different components of electric and magnetic fields in order to understand the nature of the disturbances described above.

Figure 5 shows the Fourier analysis of $Ey(x/d_i = 9.3, y/d_i(0 : 18.5))$ perpendicular to the initial magnetic field, during $t\omega_{\rm pe} = (0–1500)$ in terms of $\omega/\omega_{\rm pe}$ and $k_y d_i$. The dotted/solid lines again indicate the theoretical modes propagating perpendicular to the initial magnetic field. According to this graph, only the X-mode (extraordinary mode) accompanied by magnetosonic waves is excited. The cutoffs of the X-mode are the same as R and L mode cutoffs. The dispersion relation of magnetosonic wave perpendicular to the magnetic field line reduces to $\omega = k_y\sqrt{C_s^2 + V_A^2}$, with the sound speed

https://doi.org/10.1017/S0022377821001367 Published online by Cambridge University Press

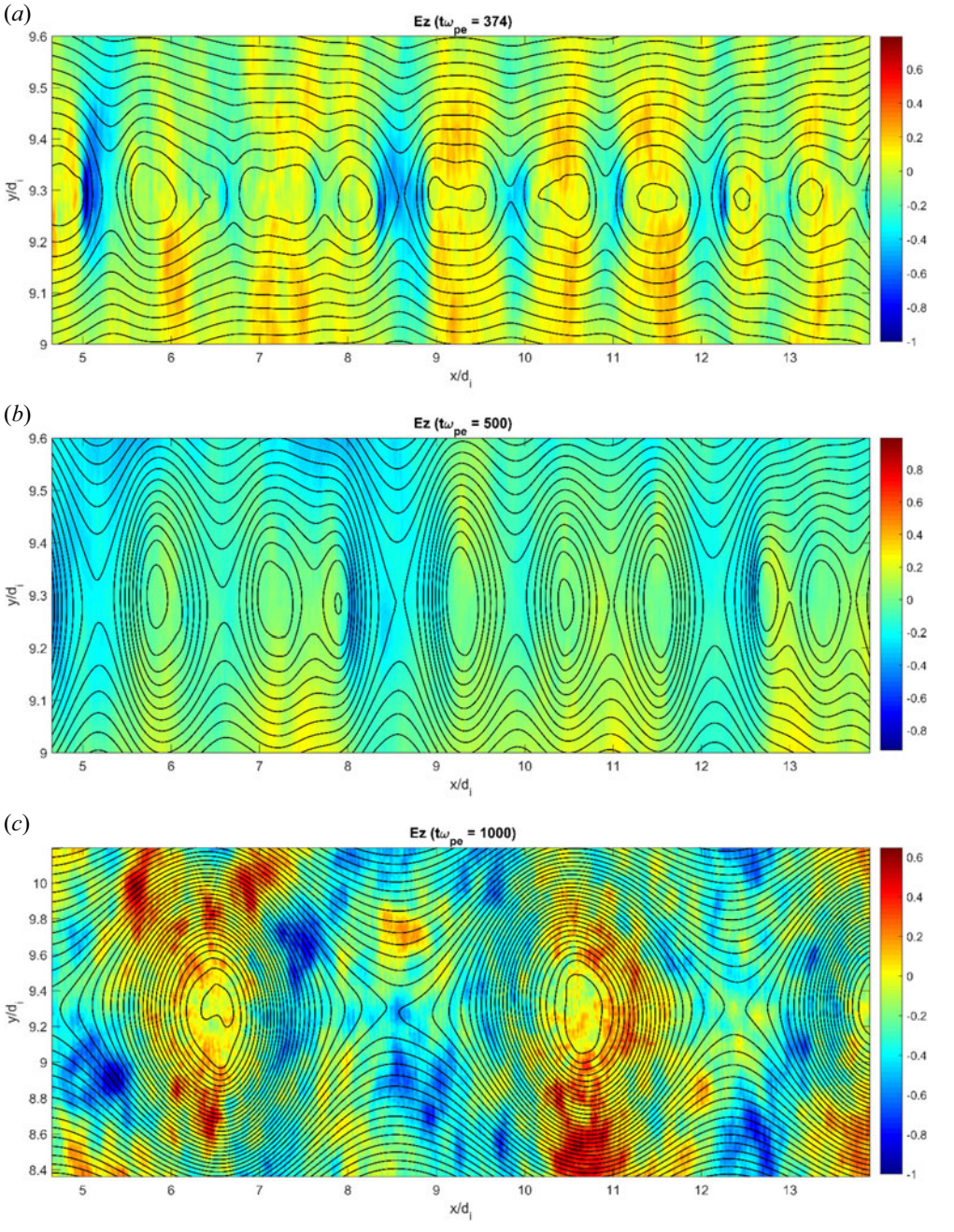


FIGURE 4. Zoomed-in plots of E_z at times $t\omega_{\rm pe} = 374$ (a), 500 (b) and 1000 (c) with $b_{z0} = 0.3B_0$.

$C_s = \sqrt{(KT_e + \gamma KT_i)/m_i} \sim 7 \times 10^5$ ms^{-1} and the Alfvén velocity $V_A = B_0/\sqrt{\mu_0 n_i m_i} \sim 3 \times 10^7$ ms^{-1}. Since $V_A^2 \gg C_s^2$, the dispersion relation takes the form $\omega \sim k_y V_A$, i.e. $\omega/\omega_{\rm pe} = 0.01(k_y d_i)$. The slope of the line specified by the 'magnetosonic wave' in figure 5 is 0.008. Taking into account the slope of the theoretical dispersion relation,

https://doi.org/10.1017/S0022377821001367 Published online by Cambridge University Press

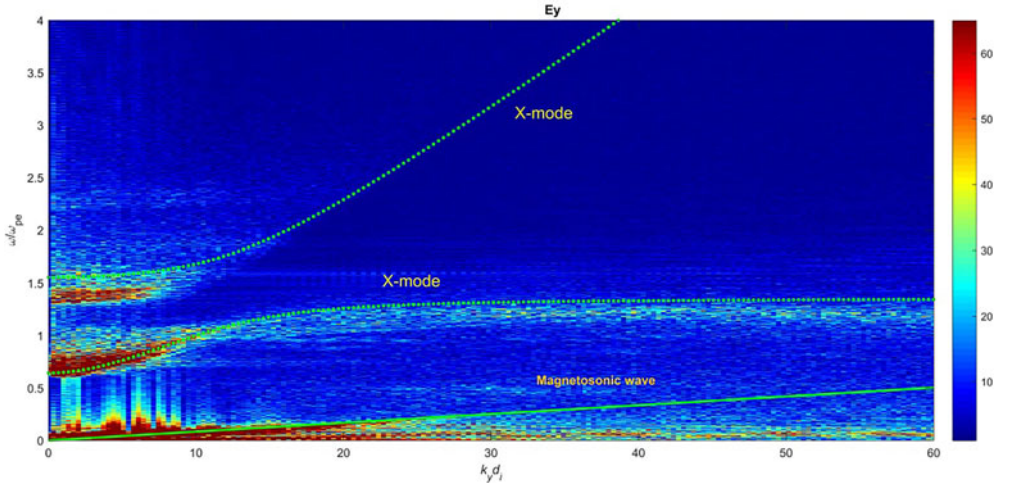


FIGURE 5. Dispersion diagram of $Ey(x/d_i = 9.3, y/d_i(0 : 18.5))$. Dotted lines indicate the theoretical parallel propagating modes along the initial magnetic field.

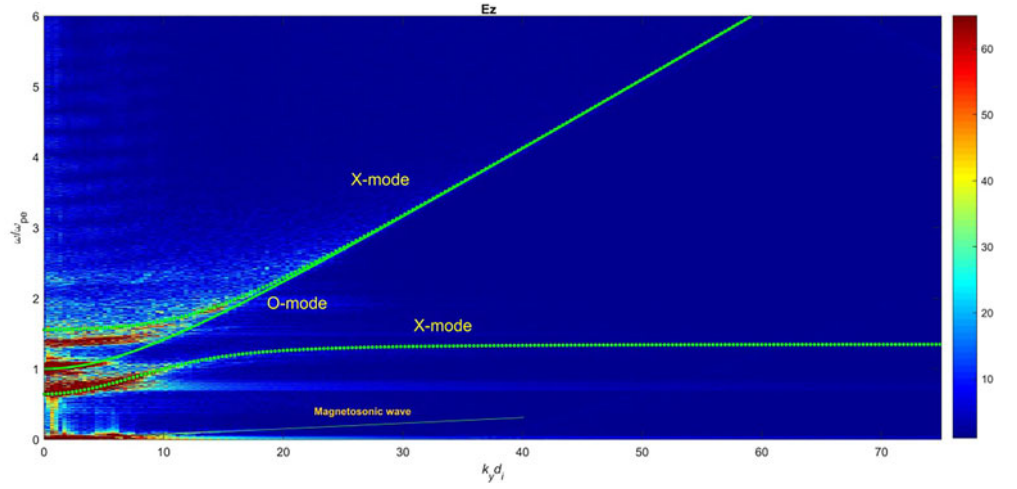


FIGURE 6. Dispersion diagram of $Ez(x/d_i = 10.2, y/d_i(0 : 18.5))$. Bold lines indicate the theoretical parallel propagating modes along the initial magnetic field.

0.010, we can conclude that the respective mode is the magnetosonic waves propagating perpendicular to the magnetic field. Additionally, it seems that at very small frequencies $\omega/\omega_{pe} < 1$, ion-sound wave with a frequency of the order of $\omega_{pi} = 0.1\omega_{pe}$ is excited. The corresponding theoretical dispensation relation is $\omega = k_y C_s$, i.e. $\omega/\omega_{pe} = 0.0002(k_y d_i)$, and, as seen, the dispersion diagram of the ion-sound wave has a very small group velocity.

Finally, the Fourier analyses of $Ez(x/d_i = 10.2, y/d_i(0 : 18.5))$ and $Ez(x/d_i(0 : 18.5), y/d_i = 13)$ during $t\omega_{pe} = (0–1500)$ are shown in figures 6 and 7. The parallel and perpendicular modes detected here are the same modes discussed already.

So far, we have discussed the results for Run A. A similar scenario of plasmoid instability also develops for Runs B and C. Figures 8 and 9 show J_z at time $t\omega_{pe} = 1500$. In Runs B and C, we observe the same types of different-mode disturbances, inferring that

https://doi.org/10.1017/S0022377821001367 Published online by Cambridge University Press

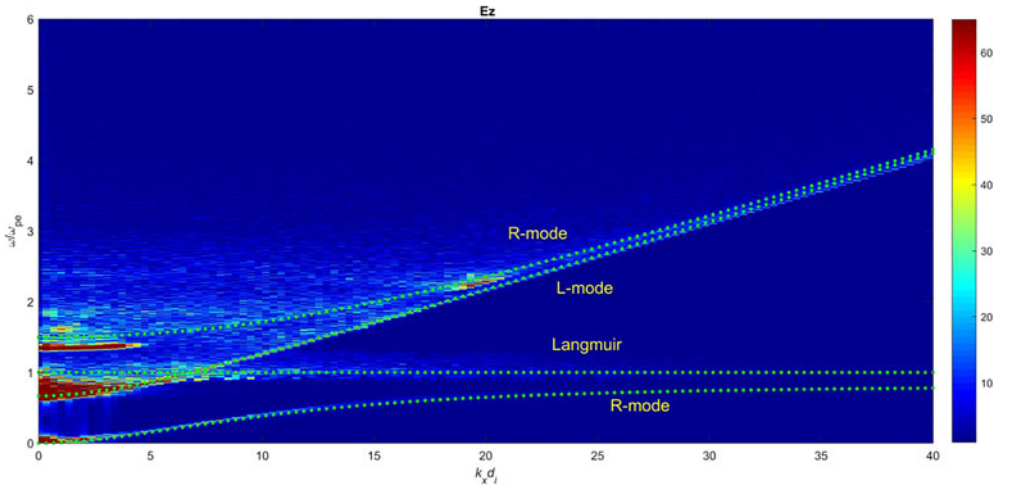


FIGURE 7. Dispersion diagram of $Ez(x/d_i(0:18.5), y/d_i = 13)$. Bold lines indicate the theoretical parallel propagating modes along the initial magnetic field.

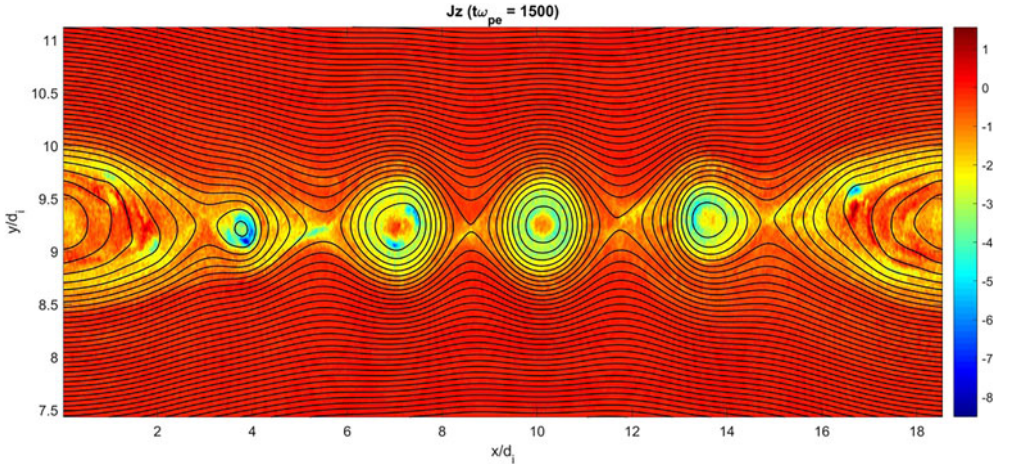


FIGURE 8. Perpendicular component of the electric current density J_z being superimposed by the magnetic field lines at time $t\omega_{\rm pe} = 1500$ for $b_{z0} = 0.5B_0$.

their nature is independent of the magnitude of the guide field. To get this conclusion, another run was done with a zero guide field, $b_{z0} = 0$, and still similar disturbances were generated. According to the presented results (figures 8 and 9), as the amplitude of the guide field increases, the number of plasmoids generated initially decreases and the growth rate of instability is slow. This fact results in the larger-size magnetic islands in the case $b_{z0} = 0.5B_0$ (figure 8) compared with the case $b_{z0} = 0.7B_0$ (figure 9) at the same time $t\omega_{\rm pe} = 1500$. Moreover, as seen from figure 9, the plasmoid-dominated layer becomes asymmetric as the guide field increases. The asymmetry of the current layer can be even seen from figure 8.

As a final point to make, variation of guide field amplitude has a significant effect on the electric field energy. Figure 10 plots the reconnection-plane electric energy density, $1/2\epsilon_0(E_x^2 + E_y^2)$, which is normalized to the initial reconnection-plane magnetic

https://doi.org/10.1017/S0022377821001367 Published online by Cambridge University Press

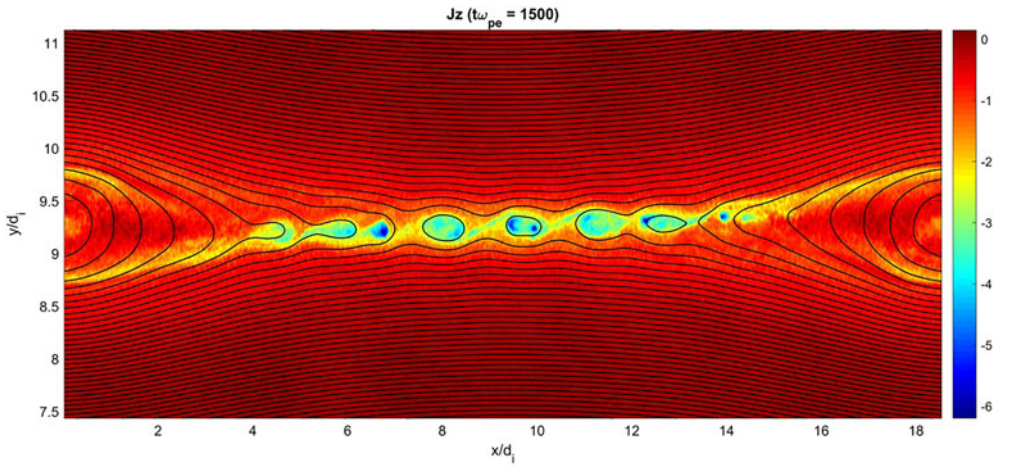


FIGURE 9. Perpendicular component of the electric current density J_z being superimposed by the magnetic field lines at time $t\omega_{pe} = 1500$ for $b_{z0} = 0.7B_0$.

energy density $(B_x^2(t=0) + B_y^2(t=0))/2\mu_0$. As seen from figure 10, up to time $t\omega_{pe} \sim 200$, the electric field energy oscillates for all three Runs A, B and C due to the electromagnetic/electrostatic waves propagating away from the current sheet which have already been discussed. For $t\omega_{pe} > 200$, however, behaviour is different for the three runs. For Run A, transition of magnetic reconnection into the plasmoid instability takes place faster and reconnection occurs in more than one X-point. As a result, the amplitude of reconnection-generated electric field increases. Note that small-amplitude oscillations still exist there for $t\omega_{pe} > 200$ due to the electromagnetic/electrostatic waves, the amplitude of which has been decreased compared with that at the initial times. However, for Runs B and C, the growth of plasmoid instability is relatively slow, and so the electric energy is varying slowly. As the guide field amplitude increases, the growth rate of plasmoid instability decreases. This point can also be deduced from figure 11 which shows the temporal variation of reconnection-plane magnetic energy $(B_x^2 + B_y^2)/B_0^2$ for the three runs. Obviously, a reconnection with a smaller guide field proceeds faster into the plasmoid instability. Additionally, figure 12 shows that a small-amplitude guide field leads to a larger electric field energy, E_z^2, and this is again due to the higher growth rate of the plasmoid instability.

4. Summary and conclusion

In this study, two-dimensional particle-in-cell simulation was carried out to investigate the spatial and temporal variation of electric field generated during collisionless magnetic reconnection which later transits into the plasmoid instability. The initial magnetic field is a Harris sheet superimposed by a non-uniform guide field. The input parameters are applicable for the solar corona, in the region where $\omega_{pe} > \omega_{ce}$ is justified. Three runs were done with three different amplitudes of guide field, all three smaller than the amplitude of the initial magnetic field (i.e. weak and medium guide field). For all cases, the onset of collisionless magnetic reconnection in a specified X-point is fast. By setting appropriately a large L_x/δ ratio, the reconnection, consequently, proceeds into the well-known plasmoid instability in which the current sheet is fragmented by formation of multiple secondary X-points/magnetic islands. The results showed that as the amplitude of the guide field increases, the growth rate of magnetic reconnection in the initial X-point and the plasmoid

https://doi.org/10.1017/S0022377821001367 Published online by Cambridge University Press

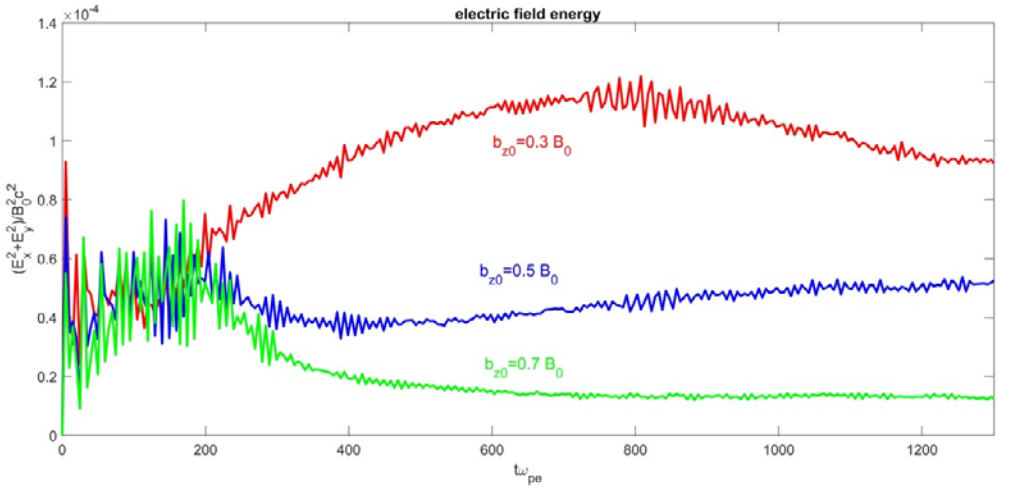


FIGURE 10. Time variation of the electric energy $(E_x^2 + E_y^2)$ for different guide field amplitudes.

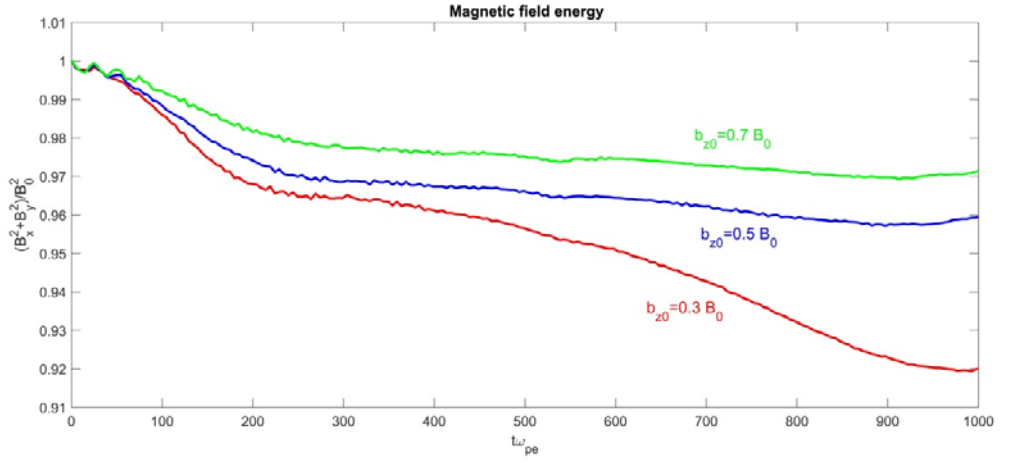


FIGURE 11. Time variation of the magnetic energy $(B_x^2 + B_y^2)$ for different guide field amplitudes.

instability decreases. This can be inferred from the slope of temporal variation of magnetic field energy (figure 11). The growth rate of reconnection at $\sim 50 < t\omega_{\rm pe} <\sim 200$ decreases by almost half as the guide field amplitude increases from $0.3B_0$ to $0.7B_0$. The results show that when a secondary X-point emerges, then the rate of magnetic energy release increases momentarily, and subsequently the electric field energy increases. Therefore, the decreasing or increasing trend of magnetic and electric energy during the linear and nonlinear stages of the plasmoid instability is not monotonic.

As the reconnection is triggered, some electrostatic/electromagnetic waves are excited and propagate perpendicularly away from the current sheet while they are uniform in the magnetic field direction, x. Later, some waves are excited along the magnetic field direction and hence the k_x and k_y components of the wavenumber vector become comparable. Signatures of these waves are observed in all components of the electric

https://doi.org/10.1017/S0022377821001367 Published online by Cambridge University Press

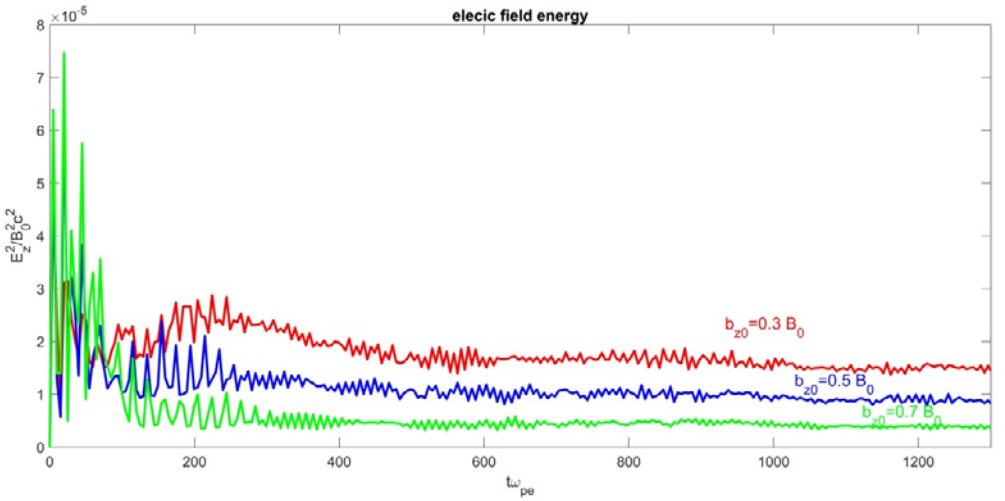


FIGURE 12. Time variation of the electric energy E_z^2 for different guide field amplitudes.

and magnetic fields. The dispersion diagrams of field components revealed that the X-mode propagates perpendicular to the magnetic field, while the R- and L-modes are the predominant modes parallel to the magnetic field. The electrostatic Langmuir and ion-related slow magnetosonic modes are also excited in both propagation directions. Parallel and perpendicular to the magnetic field, magnetosonic mode is reduced to the ion-sound and the Alfvén modes, respectively. We found that these waves are transient modes and the corresponding amplitudes of the waves decrease in time and eventually become ignorable compared with the electric field generated later by the plasmoid instability which lasts for longer times. It should be noted that the modes excited outside the current sheet are present even with the open boundary condition applied for the y axis. Following the growth of plasmoid instability and the later transition into the nonlinear stage, the associated electric field becomes stronger inside the magnetic islands and also around the separatrices compared with other places, and as time goes on, the amplitude of electric field increases. The strong electric field at longer times is favourable for accelerating charged particles to highly relativistic energies.

Considering our input parameters, the time scale of fast growth of plasmoid instability in our simulations is of the order of a few microseconds. However, for larger guide fields, the growth rate is smaller. In other words, for a reconnection with a weak guide field, transition to the plasmoid instability occurs faster and the generation of multiple secondary X-points and the size-growth of magnetic islands take place on shorter time scales. Since the X-points are the places where the magnetic energy is released due to the reconnection process, then the fast generation of such null points of many in number results in the faster reduction of magnetic energy and so the faster increase of electric energy. Furthermore, during the plasmoid instability, an out-of-plane electric field is generated which, based on our parameters, is of the order of a few kV m^{-1}. Such a strong electric field, although spatially localized around X-points, is the most suitable candidate for accelerating charged particles perpendicular to the reconnection plane. Studying the particle trajectory and acceleration in the presence of different components of the electric and magnetic fields is our next work to do. The effect of reconnection-plane electric fields and also the different amplitude guide fields on the acceleration scenario will be considered. As a final point to make, according to the presented results, the electric field components located on

https://doi.org/10.1017/S0022377821001367 Published online by Cambridge University Press

the reconnection plane can play an important role in the particle acceleration problem since their amplitude during the plasmoid instability is as large as that of the out-of-plane component. In some literature, attention is mostly paid to the out-of-plane component of the electric field.

Acknowledgments

The authors are grateful to the EPOCH code development team that allowed us use of the code for simulations.

Editor Francesco Califano thanks the referees for their advice in evaluating this article.

Funding

This research received no specific grant from any funding agency, commercial or not-for-profit sectors.

Declaration of interests

The authors report no conflict of interest.

Data availability statement

The data that support the findings of this study are available from the corresponding author upon reasonable request.

Author contributions

All authors contributed equally to performing simulations, analysing data, reaching conclusions and in writing the paper.

REFERENCES

BÁRTA, M., BÜCHNER, J., KARLICKÝ, M. & KOTRČ, P. 2011 Spontaneous current-layer fragmentation and cascading reconnection in solar flares: II. Relation to observations. *Astrophys. J.* **730**, 47.

BHATTACHARJEE, A. 2004 Impulsive magnetic reconnection in the Earth's magnetotail and the solar corona. *Annu. Rev. Astron. Astrophys*. **42**, 365.

BHATTACHARJEE, A., BRUNEL, F. & TAJIMA, T. 1983 Magnetic reconnection driven by the coalescence instability. *Phys. Fluids* **26**, 3332.

BIRN, J. & PRIEST, E. 2007 *Reconnection of Magnetic Fields: Magnetohydrodynamic and Collisionless Theory and Observations*. Cambridge University Press.

CARGILL, P.J., VLAHOS, L., BAUMANN, G., DRAKE, J.F. & NORDLUND, Å. 2012 Current fragmentation and particle acceleration in solar flares. *Space Sci. Rev*. **173**, 223.

CHEN, L.J., DAUGHTON, M., BHATTACHARJEE, A., TORBERT, R.B., ROYTERSHTEYN, V. & BESSHO, N. 2012 In-plane electric fields in magnetic islands during collisionless magnetic reconnection. *Phys. Plasmas* **19**, 112902.

COMISSO, L., LINGAM, M., HUANG, Y.-M. & BHATTACHARJEE, A. 2016 General theory of the plasmoid instability. *Phys. Plasmas* **23**, 100702.

COMISSO, L., LINGAM, M., HUANG, Y.-M. & BHATTACHARJEE, A. 2017 Plasmoid instability in forming current sheets. *Astrophys. J.* **850**, 142.

DAUGHTON, W., ROYTERSHTEYN, V., ALBRIGHT, B.J., KARIMABADI, H., YIN, L. & BOWERS, K.J. 2009 Role of electron physics in the development of turbulent magnetic reconnection in collisionless plasmas. *Phys. Rev. Lett*. **103**, 065004.

DRAKE, J.F., SWISDAK, M., SCHOEFFLER, K.M., ROGERS, B.N. & KOBAYASHI, S. 2006 Formation of secondary islands during magnetic reconnection. *Geophys. Res. Lett*. **33**, L13105.

EGEDAL, J., DAUGHTON, W. & LE, A. 2012 Large-scale electron acceleration by parallel electric fields during magnetic reconnection. *Nat. Phys*. **8**, 321.

https://doi.org/10.1017/S0022377821001367 Published online by Cambridge University Press

FAN, F., HUANG, C., LU, Q., XIE, J. & WANG, S. 2016 The structures of magnetic islands formed during collisionless magnetic reconnections in a force-free current sheet. *Phys. Plasmas* **23**, 112106.

FU, S., HUANG, S., ZHOU, M., NI, B. & DENG, X. 2018 Tripolar electric field structure in guide field magnetic reconnection. *Ann. Geophys*. **36**, 373.

GALSGAARD, K. & NORDLUND, Å. 1996 Heating and activity of the solar corona: 1. Boundary shearing of an initially homogeneous magnetic field. *J. Jnobreak Geophys. Res*. **101**, 13445.

GONZALEZ, W. & PARKER, E. 2016 *Magnetic Reconnection Concepts and Applications*. Springer.

GUDIKSEN, B.V. & NORDLUND, Å. 2005 An ab initio approach to the solar coronal heating problem. *Astrophys. J*. **618**, 1020.

INTRATOR, T.P., SUN, X., LAPENTA, G., DORF, L. & FURNO, I. 2009 Experimental onset threshold and magnetic pressure pile-up for 3D reconnection. *Nat. Phys*. **5**, 521.

KARIMABADI, H., DORELLI, J., ROYTERSHTEYN, V., DAUGHTON, W. & CHACON, L. 2011 Flux pileup in collisionless magnetic reconnection: bursty interaction of large flux ropes. *Phys. Rev. Lett*. **107**, 025002.

KARIMABADI, H., KRAUSS-VARBAN, D. & OMIDI, N. 1999 Magnetic structure of the reconnection layer and core field generation in plasmoids. *J. Jnobreak Geophys. Res*. **104**, 12313.

KUMAR, P., KARPEN, J.T., ANTIOCHOS, S.K., WYPER, P.F. & DEVORE, C.R. 2019 First detection of plasmoids from breakout reconnection on the Sun. *Astrophys. J. Lett*. **885**, L15.

LIU, W., CHEN, Q. & PETROSIAN, V. 2013 Plasmoid ejections and loop contractions in an eruptive M7.7 solar flare: evidence of particle acceleration and heating in magnetic reconnection outflows. *Astrophys. J*. **767**, 168.

LOUREIRO, N.F., SCHEKOCHIHIN, A.A. & COWLEY, S.C. 2007 Instability of current sheets and formation of plasmoid chains. *Phys. Plasmas* **14**, 100703.

MARKIDIS, S., HENRI, P., LAPENTA, G., DIVIN, A., GOLDMAN, M.V., NEWMAN, D. & ERIKSSON, S. 2012 Collisionless magnetic reconnection in a plasmoid chain. *Nonlinear Process. Geophys*. **19**, 145.

PRIEST, E. & FORBES, T. 2000 *Magnetic Reconnection: MHD Theory and Applications*. Cambridge University Press.

WAN, W., LAPENTA, G., DELZANNO, G.L. & EGEDAL, J. 2008 Electron acceleration during guide field magnetic reconnection. *Phys. Plasmas* **15**, 032903.

YAMADA, M., KULSRUD, R. & JI, H. 2010 Magnetic reconnection. *Rev. Mod. Phys*. **82**, 603.

ZHOU, M., DENG, X.H. & HUANG, S.Y. 2012 Electric field structure inside the secondary island in the reconnection diffusion region. *Phys. Plasmas* **19**, 042902.

https://doi.org/10.1017/S0022377821001367 Published online by Cambridge University Press